INTERNATIONAL ATOMIC ENERGY AGENCY
UNITED NATIONS EDUCATIONAL, SCIENTIFIC AND CULTURAL ORGANIZATION
INTERNATIONAL CENTRE FOR THEORETICAL PHYSICS
I.C.T.P., P.O. BOX 586, 34100 TRIESTE, ITALY, CABLE: CENTRATOM TRIESTE

UNITED NATIONS INDUSTRIAL DEVELOPMENT ORGANIZATION
INTERNATIONAL CENTRE FOR SCIENCE AND HIGH TECHNOLOGY

H4.SMR/540-11

Second Training College on Physics and Technology of Lasers and Optical Fibres

21 January - 15 February 1991

OPTOGALVANIC SPECTROSCOPY II

E. Arimondo
Università di Pisa
Dipartimento di Fisica
Pisa, Italy

Mechanisms of Optogalvanic and Optoacoustic in Discharges

by

Ennio Arimondo
Dipartimento di Fisica
Università di Pisa
Italy

Optogalvanic Spectroscopy

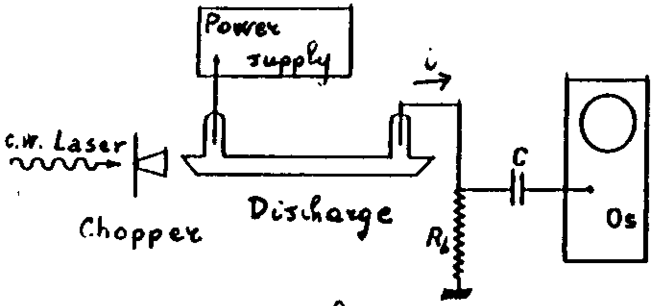

in low power discharge tubes

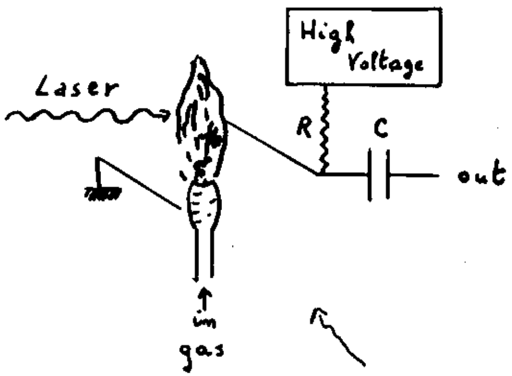

in flames

Review papers on optogalvanic:

V. N. Ochkin, N. G. Preobrazhenskii, N. N. Sobolev and N. Ya. Shaparev

Sov. Phys. Usp. 29 260 (1986)

B. Barbieri, N. Beverini and A. Sasso

Rev. Mod. Phys. 62 603 (1990)

OG spectroscopy in flames:

hydrogen photoionization

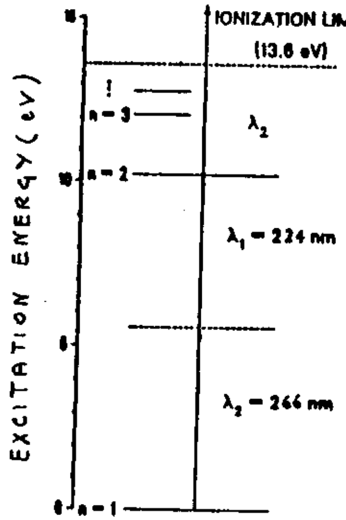

50 mJ

dye laser frequency doubled and mixed with Nd:YAG

50 mJ

hydrogen spectrum

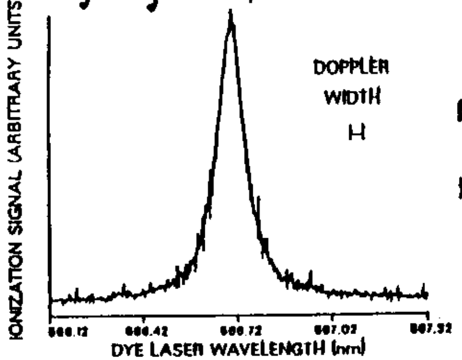

hydrogen/oxygen premixed flame

(J. E. Goldsmith, Sandia Laboratories, Opt. Lett. 7 437 (1982))

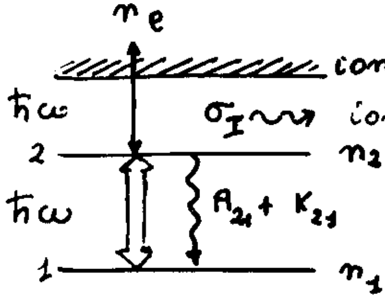

laser fluence $h\nu\phi$ [per unit area]

flux $h\nu F$ [per unit area]

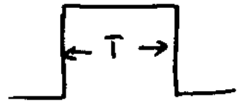

laser pulse

$\phi = FT$

Rate equations for photoionization

$n_1(t) = n_2(t)$ $\qquad$ $n_1(0) + n_2(0) = n_T$

$$\frac{dn_2}{dt} = -\sigma_I F n_2(t) - (A_{21} + K_{21})\, n_2(t)$$

$$n_e(T) = \int_0^T \sigma_I F n_2(t)\, dt =$$

$$= \frac{\sigma_I F n_T}{\sigma_I F + A_{21} + K_{21}} \left\{ 1 - e^{-(\sigma_I F + A_{21} + K_{21})T} \right\}$$

Conditions

$\sigma_I F T = \sigma_I \phi \gg 1$

$\sigma_I F \gg A_{21} + K_{21}$

Summary

OG signal: collection and ionization

OG mechanisms:

- photoionization
- collisional ionization
- associative "
- state dependent mobility
- cathode surface collisions
- electronic and atomic temperatures
- ? in Rydberg states

OG and OA simultaneous detection
in atoms and molecules
power balance

Discharge

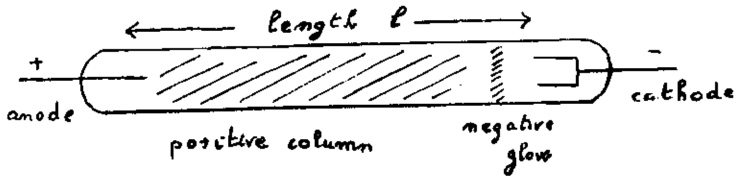

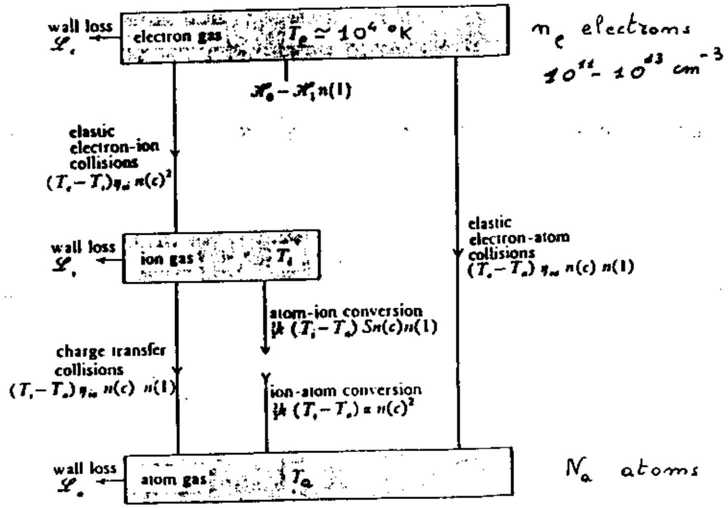

Discharge features:

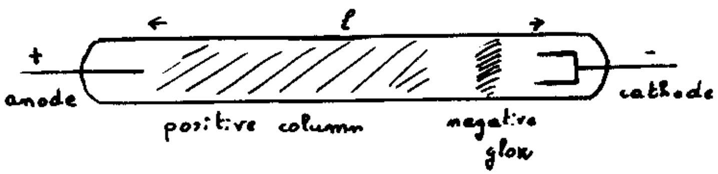

discharge parameters

E electric field

T_e electron temperature ~ 10^4 °K
(>> gas temperature T_g)

T_a atomic excitation temperature ($\leq T_e$)

n_e electron density ($10^{11} - 10^{13}$ cm^{-3})

μ_e electron mobility

μ_i ion mobility

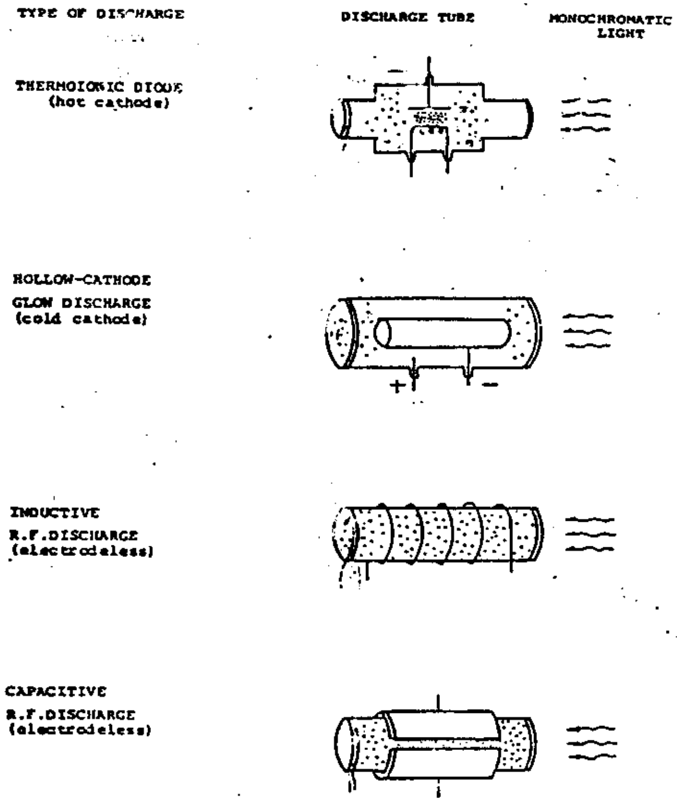

Fig. 3 Gas discharge plasmas investigated by optical impedance spectroscopy

Current equation

$$i = F(n_e, E)$$

(for instance positive column $i = e\pi R^2 v_d n_e 2h_0$)

In the optogalvanic effect the measured current change Δi_{OG} produced by Ω photons absorbed per unit time may be written:

$$\Delta i_{OG} = e_i \, e_c \, \Omega$$

$$e_c = \frac{\frac{dV}{di}}{R_b + \frac{dV}{di}}$$

depends on (V, i) characteristics of discharge and ballast resistor R_b

collection efficiency

e_i = (ion production) * (discharge perturbation)

depends on physical processes involved in ionization

ionization efficiency

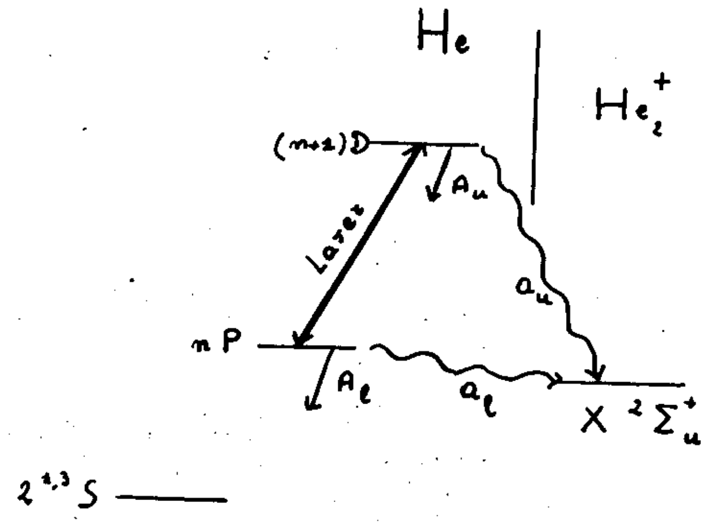

Examples

$He(2^3P) + 587.6\,nm \rightarrow He(3^3D)$

(Lawler, Phys. Rev. A22 1025 (1980))

$He(n=4) + 3\,\mu m \rightarrow He(n=6)$

(D. Jackson, E. A. et al, Opt. Comm. 33 51(1980))

Ionization efficiency : $He^* + He(1^1S_0) \xrightarrow{a} He_2^+ + e^-$

$$e_i = \left(\frac{a_u}{a_u + A_u} - \frac{a_e}{a_e + A_e} \right) \cdot \frac{e R v_d}{s_0 \ell \left(\frac{2kT_e}{m_i} \right)^{1/2}}$$

Optogalvanic model for He discharge

n_e electron density $\qquad n_e = N_i$

N_i ion density

→ Ion production through two-step electron impact:

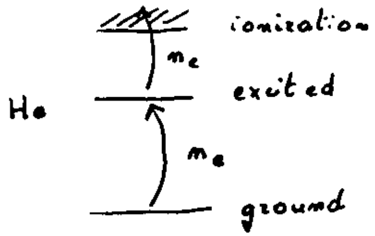

→ Equation for ion current

$$\frac{d(eN_iV)}{dt} = g(E)\,n_e^2 - \left(\frac{2kT_e}{m_i}\right)^{1/2} n_e\, 2\pi R l s_0 h_0$$

$$= G(n_e, E) = 0$$

V = volume

R = radius

l = length

E: Electric field

T_e = electron temperature

s_0, h_0 = constants

→ Equation for current

$$i = e n_e v_d \pi R^2 2h_0 = e n_e \mu E \pi R^2 2h_0$$

$$= F(n_e, E)$$

v_d = drift velocity

μ = electron mobility

Perturbed discharge:

$$\Delta i = \frac{\partial F}{\partial n_e}\Delta n_e + \frac{\partial F}{\partial E}\Delta E$$

$$\frac{d(eN_iV)}{dt} = G(n_e + \Delta n_e, E + \Delta E) + \frac{a}{A}\Omega = 0$$

$$= \underbrace{G(n_e, E)}_{=\,0} + \frac{\partial G}{\partial n_e}\Delta n_e + \frac{\partial G}{\partial E}\Delta E + \frac{a}{A}\Omega$$

Δi and ΔE not independent variables

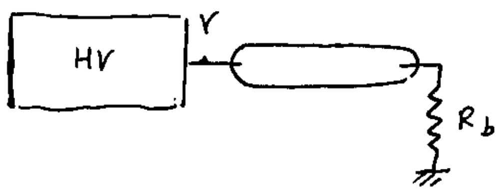

$$V = lE + iR_b + V_c \;\Big\|\; l\Delta E + R_b\Delta i = 0$$

Final result:

$$\Delta i = - \frac{a}{A} Q \frac{l}{R_b} \frac{\dfrac{\partial F}{\partial n_e}}{\dfrac{\partial G}{\partial n_e}\left(\dfrac{\partial F}{\partial E} + \dfrac{l}{R_b}\right) - \dfrac{\partial G}{\partial E}\dfrac{\partial F}{\partial n_e}}$$

Moreover

$$\frac{di}{dE} = \frac{\partial F}{\partial E} - \frac{\partial F}{\partial n_e}\frac{\partial G}{\partial E} \Big/ \frac{\partial G}{\partial n_e}$$

and

$$\frac{dV}{di} = l \frac{dE}{di} = \frac{l}{\dfrac{di}{dE}}$$

so that

$$\Delta i_{og} = \underbrace{\frac{\dfrac{dV}{di}}{R_b + \dfrac{dV}{di}}}_{e_c} \cdot \underbrace{\frac{e R v_d}{s_0 l \left(\dfrac{2kT_e}{m_i}\right)^{1/2}}\left(\frac{a_u}{a_u + A_u} - \frac{a_e}{a_e + A_e}\right) Q}_{e_i}$$

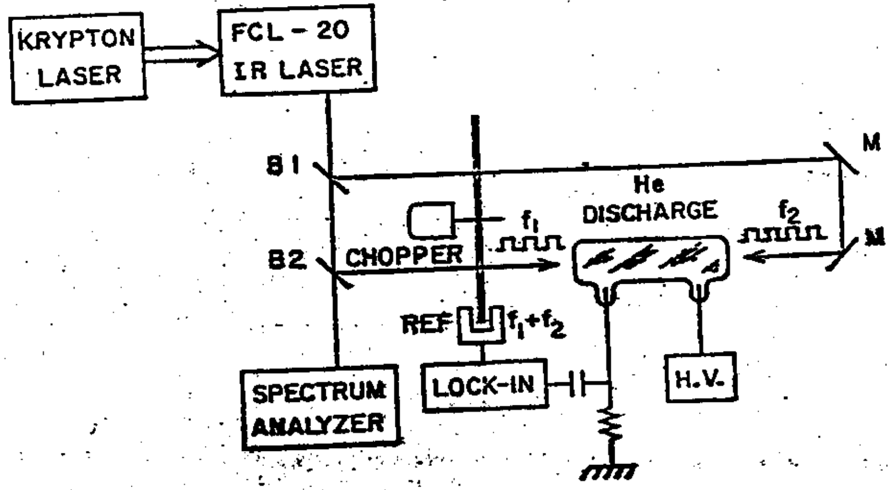

Infrared OG spectroscopy in He positive column

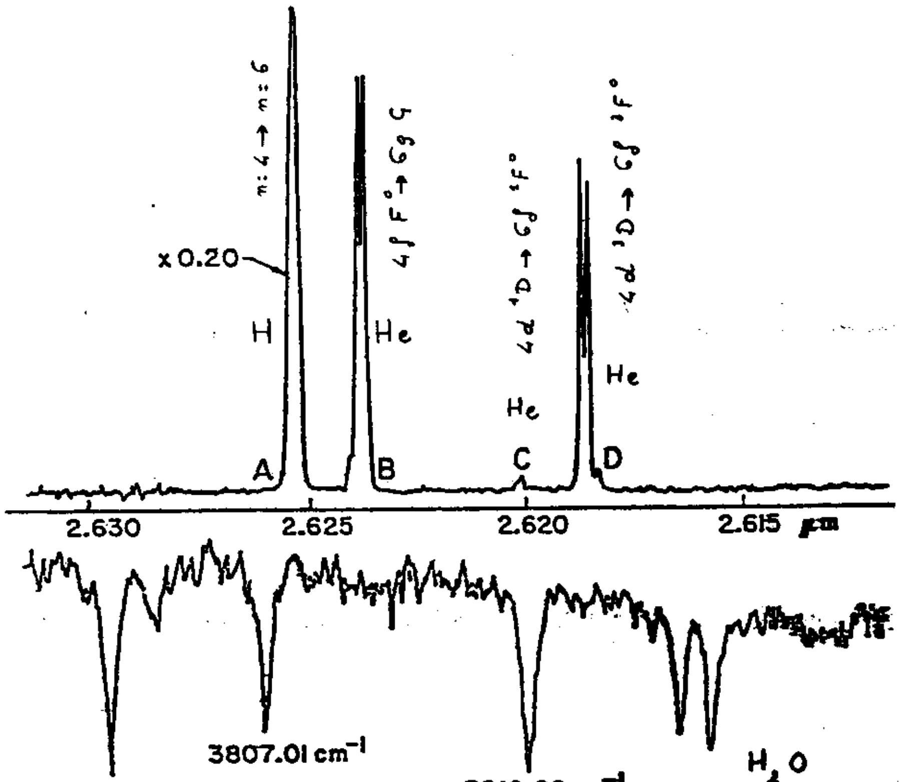

Jackson, Arimondo, Lawler, Hänsch

Opt. Commun. 33 51 (1980)

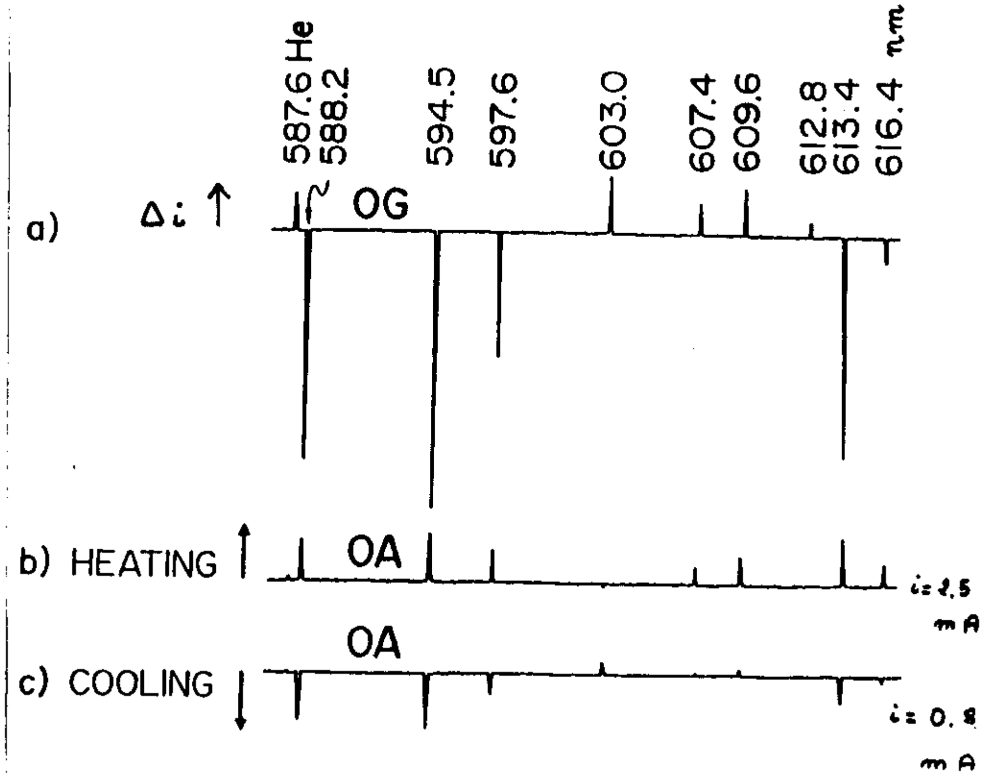

Simultaneous OG and OA observations in a He-Ne discharges (p_{Ne} = 1.2 mbars p_{He} = 2 mbars)

9

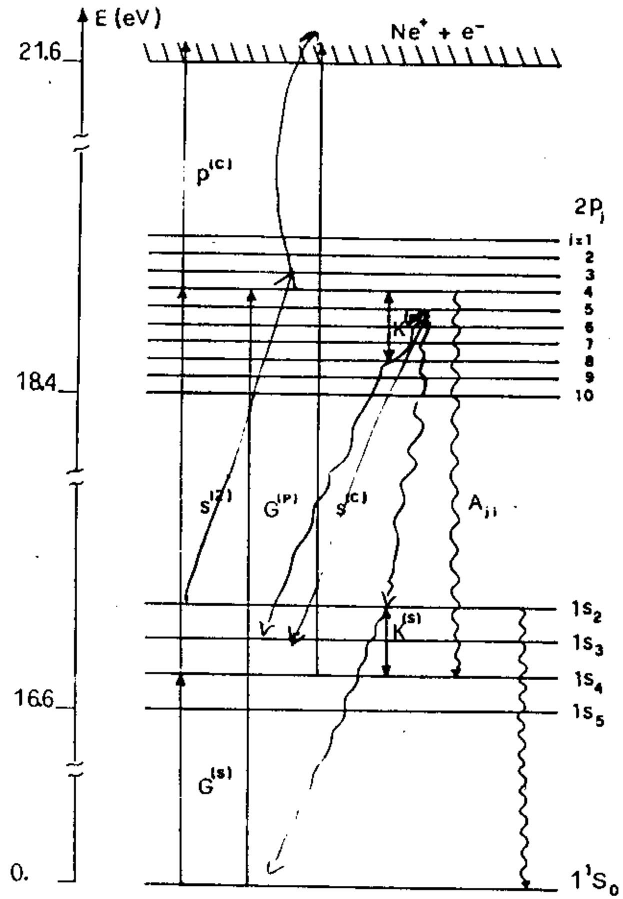

Fig. 2. Simplified energy-level diagram for neon including the $^1S_0$ ground state, the four levels $1s_i$ (i = 2, 3, 4, 5), the ten $2p_j$ levels (j = 1, 2, . . . , 10), and the continuum. The main processes of electron-impact excitation, radiative decay, and collisional mixing are schematically represented.

G, S and P processes by electron collisions

K processes by collisions with ground state neon atoms

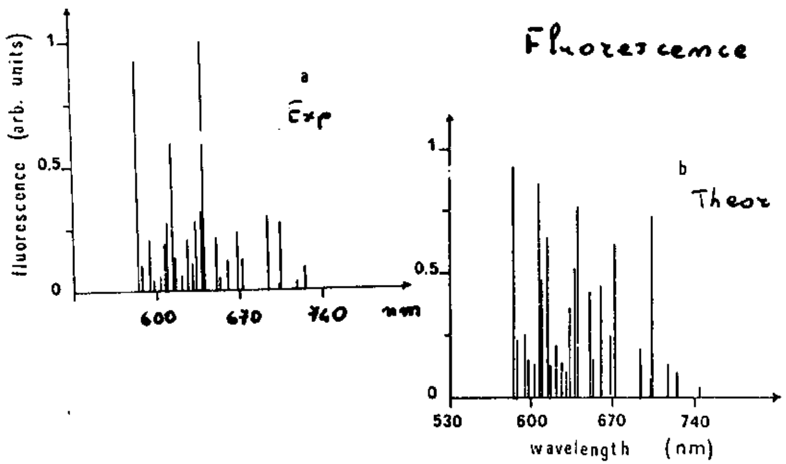

Fig. 5. Comparison between a, experimental and b, theoretical neon fluorescence spectra at 1 mA and 0.8 Torr.

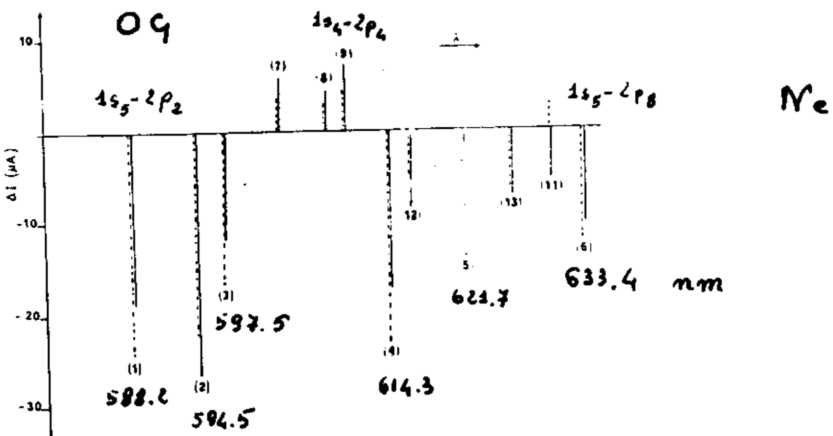

Fig. 6. Experimental (solid lines) and theoretical (dashed lines) OG spectra at 1 mA and 0.5 Torr. The laser-intensity profile in the analyzed spectral range was taken from measured intensity emission of the dye laser. The power at maximum emission (λ = 580 nm) was limited to ≈10 mW to avoid saturation for all the investigated lines. The signal represents the modification (measured in microamperes) of the current flowing through the discharge.

10

J. Opt. Soc. Amer. B5 1484 (1988)

Optogalvanic detection

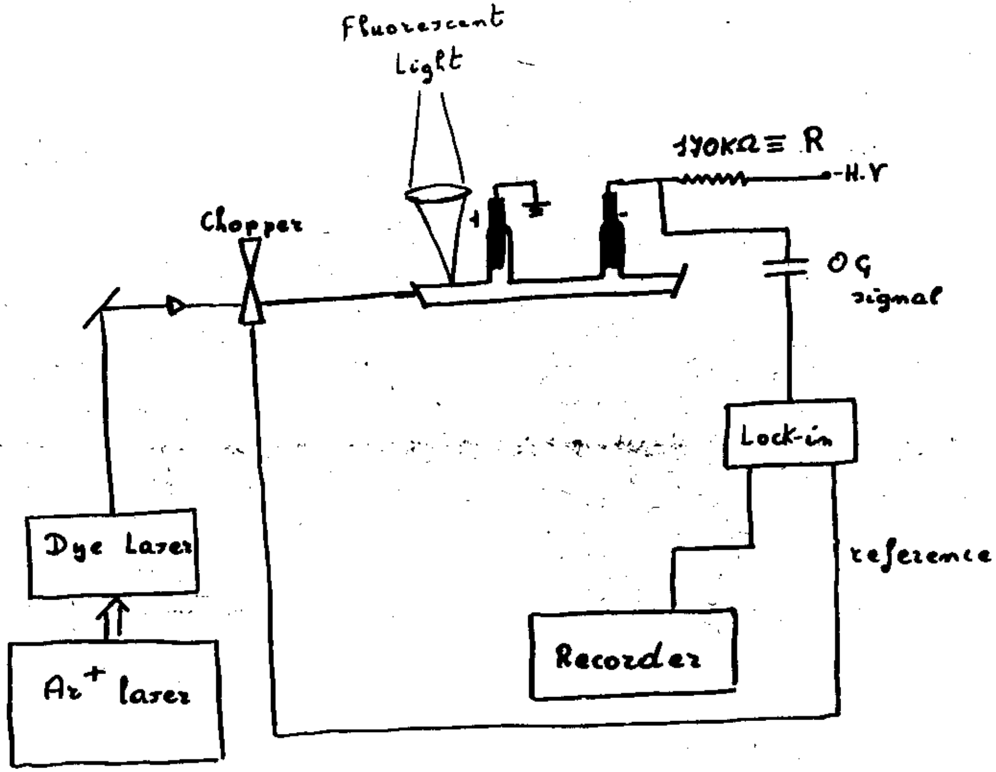

JOSA B5 1484 (1988)

Ne spectra

Sasso *et al.*

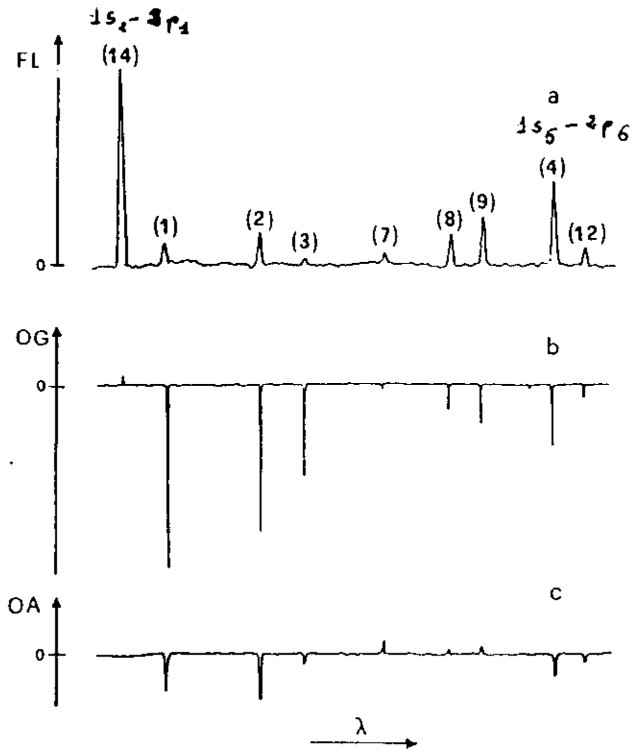

Fig. 1. Neon transitions between 580 and 620 nm observed with three different techniques: (a) the fluorescence spectrum, (b) the OG spectra and (c) the OA spectra. The spectra were recorded at 2.7-Torr neon pressure and 3-mA discharge current. The neon transitions with their assignments are listed in Table 2.

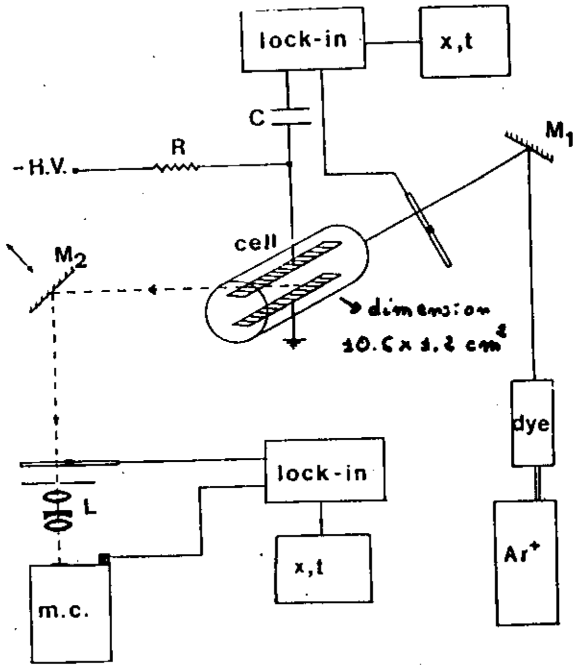

FIG. 2. Experimental setup: M1 and M2, translatable mirrors; m.c., monochromator; L, lens system; R, ballast resistor; C, coupling capacitor; x,t, chart recorder.

J. Appl. Phys. 63 649 (1988)

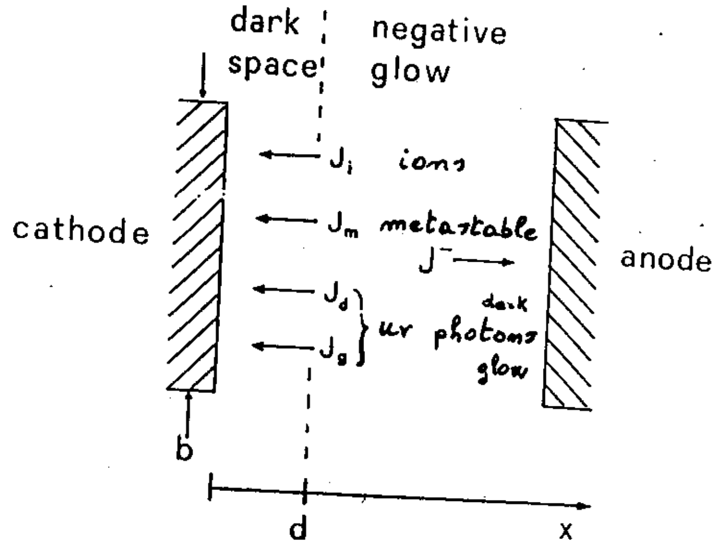

FIG. 1. Scheme of the secondary electron emission from the cathode surface.

m = metastables

n_{dark} = UV photons created dark space

n_{glow} = UV photons " glow region

12

Ne

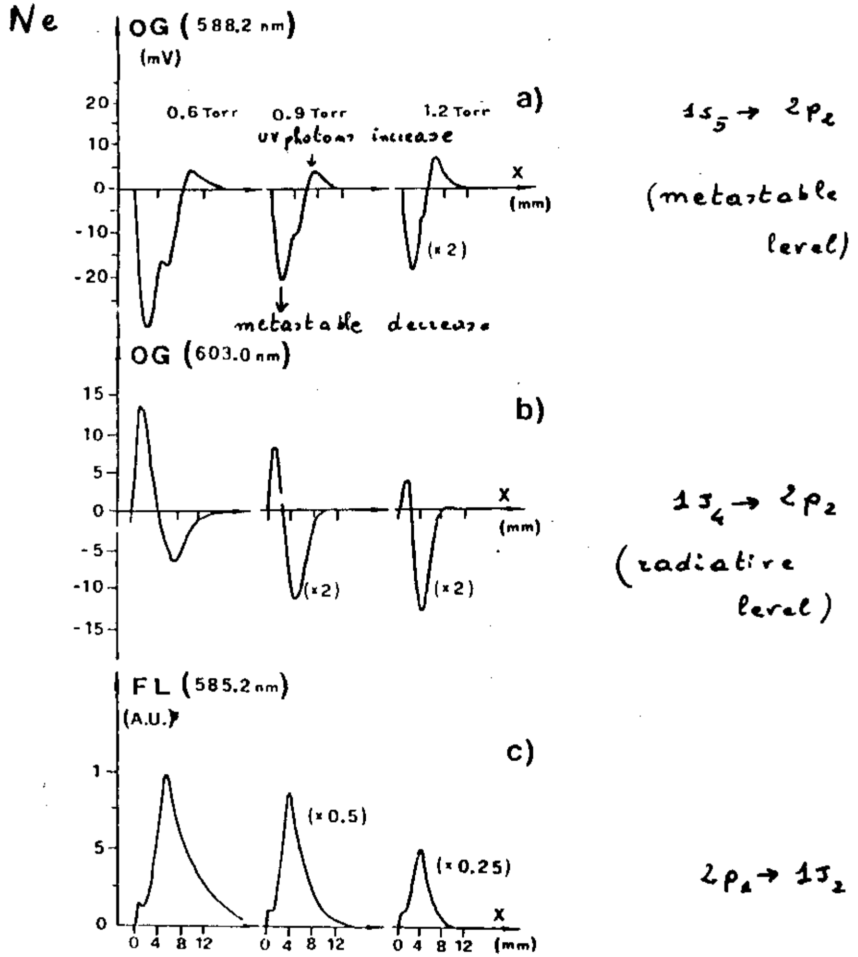

FIG. 5. Experimental OG and fluorescence signals as a function of the distance from the cathode surface: (a) OG for laser-induced excitation at 588.2 nm ($1s_5 \to 2p_2$); (b) OG for laser-induced excitation at 603.0 nm ($1s_4 - 2p_2$); (c) laser-unperturbed fluorescence from $2p_1$ to $1s_2$. The discharge current was 4 mA while 0.6, 0.9, and 1.2 Torr pressures, respectively, were used.

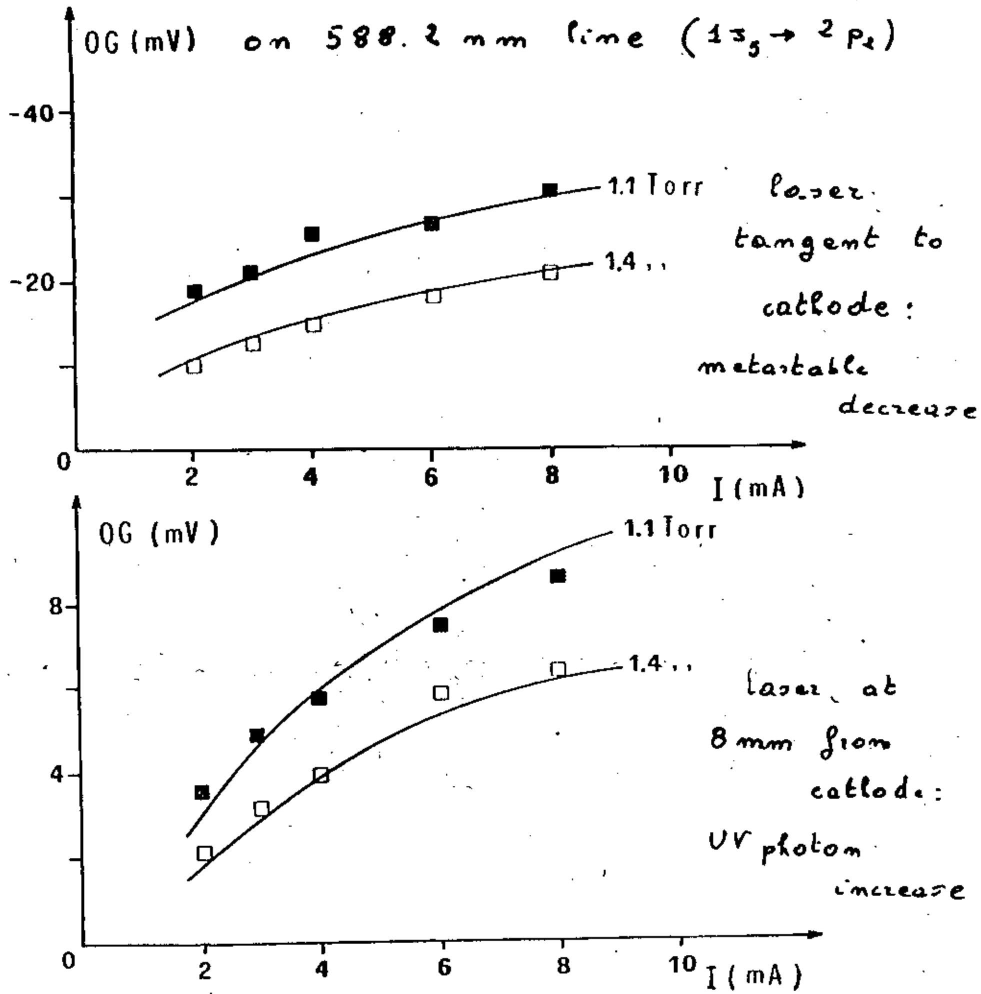

FIG. 6. OG signals vs the discharge current for 588.2 nm irradiation at two different neon pressure values, 1.1 and 1.4 Torr, respectively. (a) Laser beam tangent to the cathode surface; (b) laser beam in the region that produces the maximum OG signal. Continuous lines represent the theoretical results obtained by Eq. (13).

$$\Delta i = \frac{\partial i}{\partial m}\Delta m + \frac{\partial i}{\partial n_{dark}}\Delta n_{dark} + \frac{\partial i}{\partial n_{glow}}\Delta n_{glow}$$

DSO

N_2^+ detection

(Walkup, Dreyfus and Avouris, P.R.L. 50 1846 (1983))

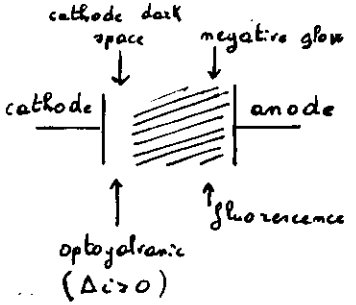

abnormal glow at 1 Torr of N_2

$X^2\Sigma_g \rightarrow B^2\Sigma_u^+$ band

N_2^+ ions have a larger mobility in the B state

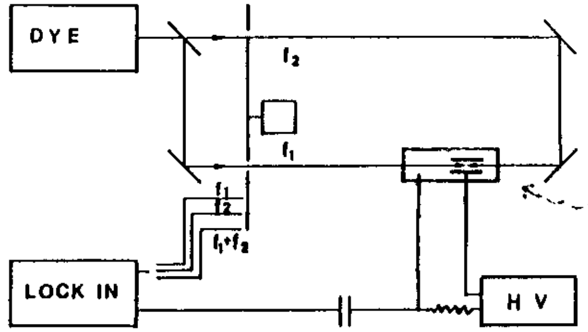

OG spectroscopy in hollow cathode discharges

Fig. 1. Schematic of the experimental apparatus used to perform Doppler limited, intermodulated Doppler-free and intermodulated Zeeman spectroscopy measurements in a hollow cathode discharge.

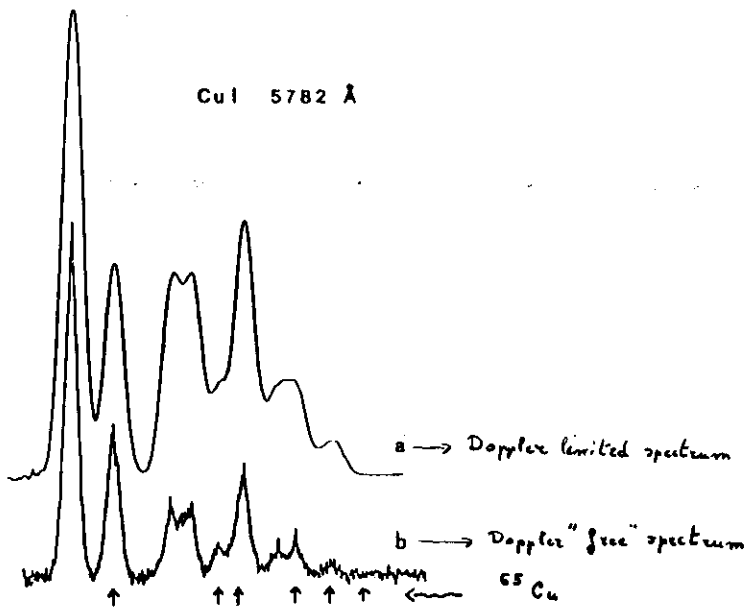

Fig. 2. Laser optogalvanic spectroscopy of the 578.2 nm transition hyperfine components of CuI. There are two naturally occurring odd isotopes. The arrows show the transitions of ^{65}Cu. (a) is a Doppler limited scan; (b) is the Doppler-free intermodulated spectrum (total frequency scan 18 GHz).

(Beverini et al, Pisa University,

In the hollow cathode discharges

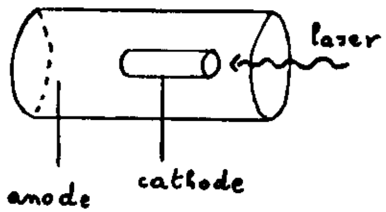

large electron density

$n_e \simeq 10^{13}\ cm^{-3}$

equal atomic and electronic temperatures $T_a \simeq T_e$

Observation of the fluorescent emission in U + Ne has shown that

• the resonant laser illumination modifies the atomic temperature,
(Dreeze et al, J. Opt. Soc. Amer. 72 912 (1982))

The OG effect arises from a change in the electron temperature, because the electron mobility in the negative glow depends on the electron temperature.
(Keller et al, J. de Physique, 44 C-7 (1983))

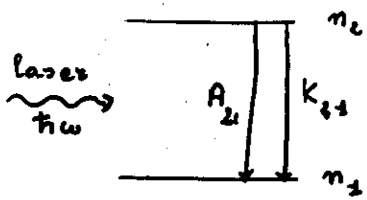

Energy released by collisions per unit time

$n_2 K_{21} \hbar\omega$

it leads to increase in temperature T

O A spectroscopy :

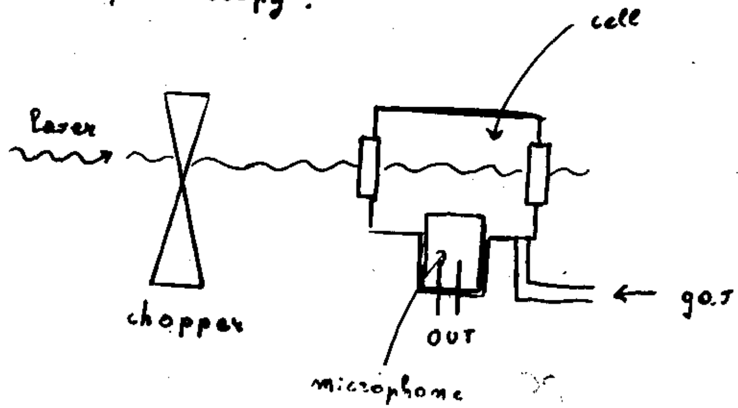

Simultaneous infrared
OG and OA on molecules

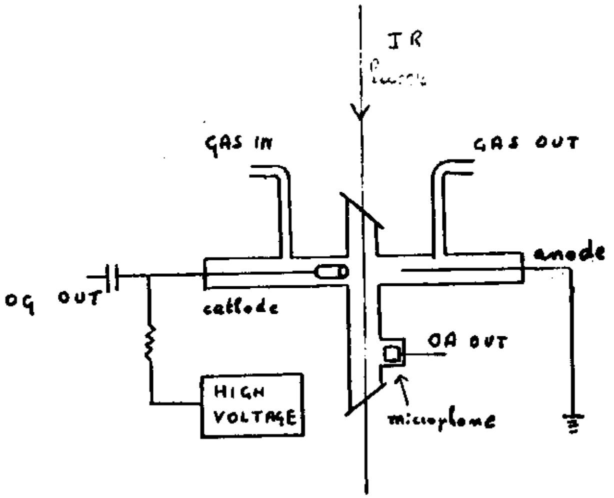

→ Optogalvanic signals produced also by irradiation outside the discharge

→ Spatial propagation with sound velocity

Hameau et al, Opt. Commun. 53 375 (1985)

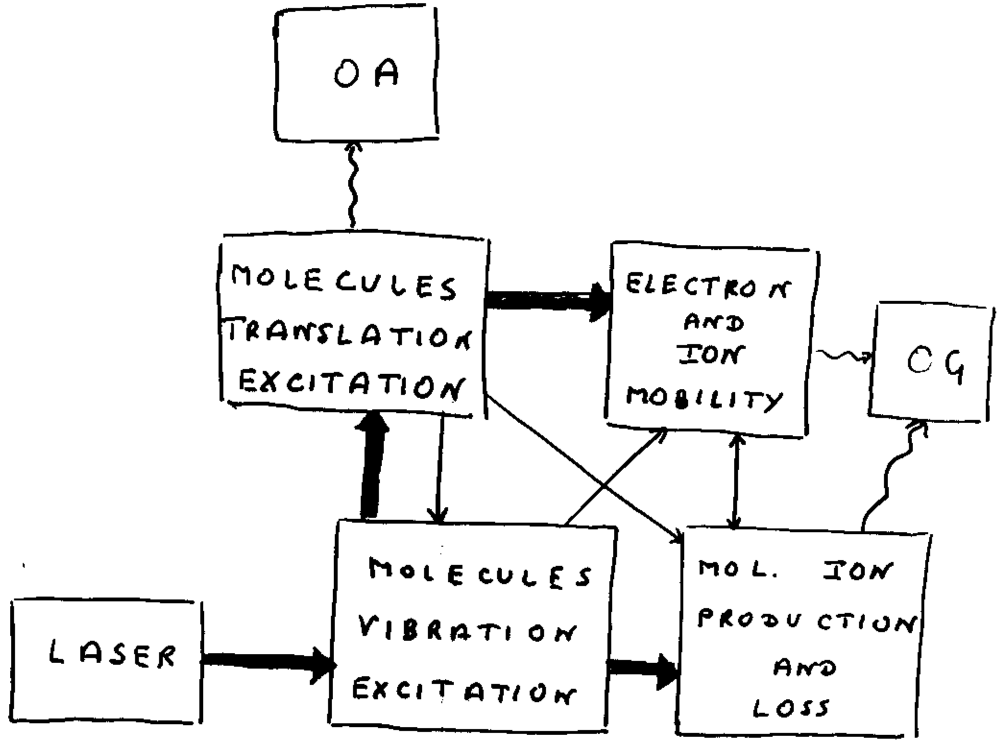

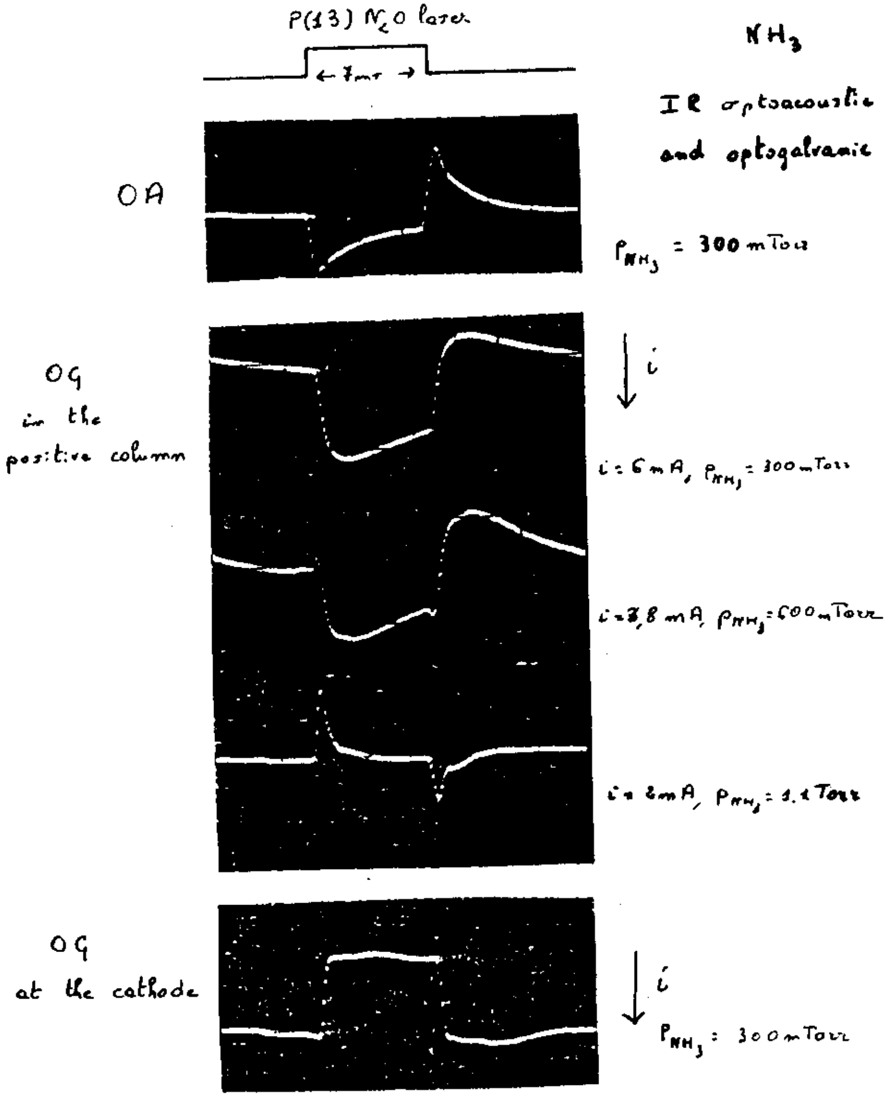

Laser : P(13) N_2O 1.3 KW

Discharge : 200 mTorr NH_3 , 3 mA

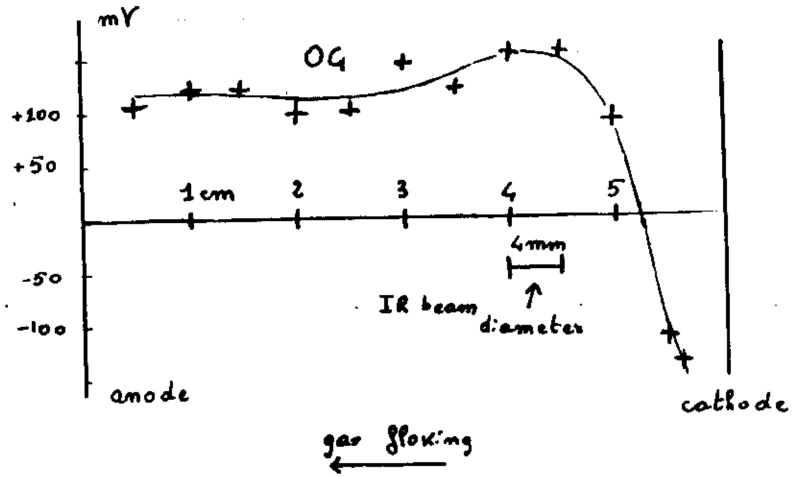

in NH_3

large elastic scattering cross sections and dissociative attachment (strongly dependent on the electric field E)

$$NH_3 + e^- \rightarrow NH_2^- + H$$

$$NH_3 + e^- \rightarrow NH^- + H_2$$

in CO_2

attachment

$$CO_2 + e^- \rightarrow CO + O^-$$

dissociation by electron impact

$$CO_2 + e^- \rightarrow CO + O + e^-$$

with cross sections smaller than the reactions in NH_3

Simultaneous optogalvanic and optoacoustic detections

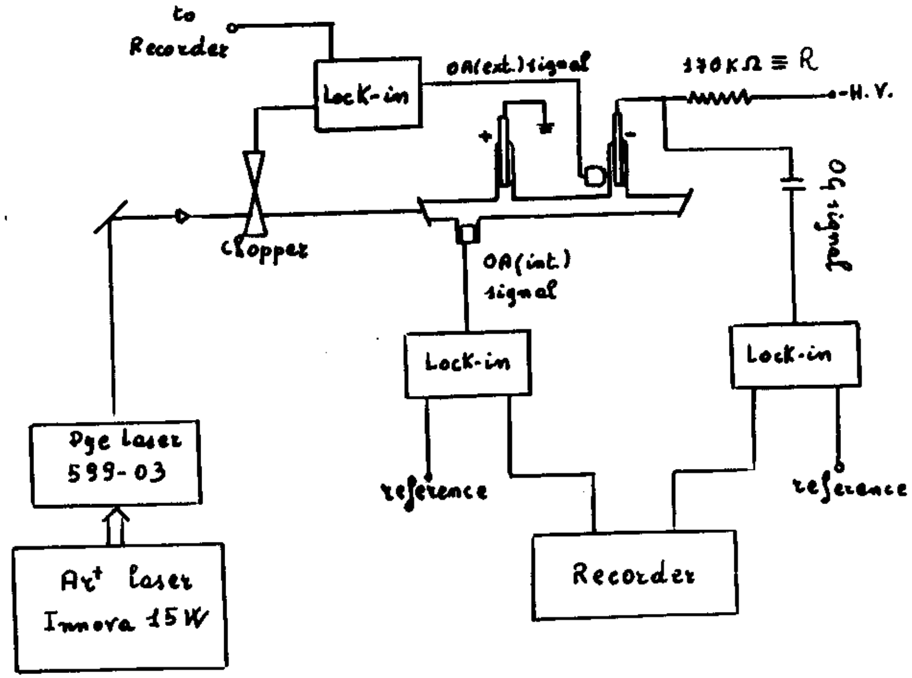

E. Arimondo, M.G. Di Vito, K. Ernst, M. Inguscio,
J. de Physique, 44 C7-267 (1983)

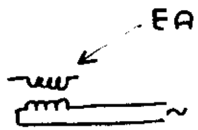

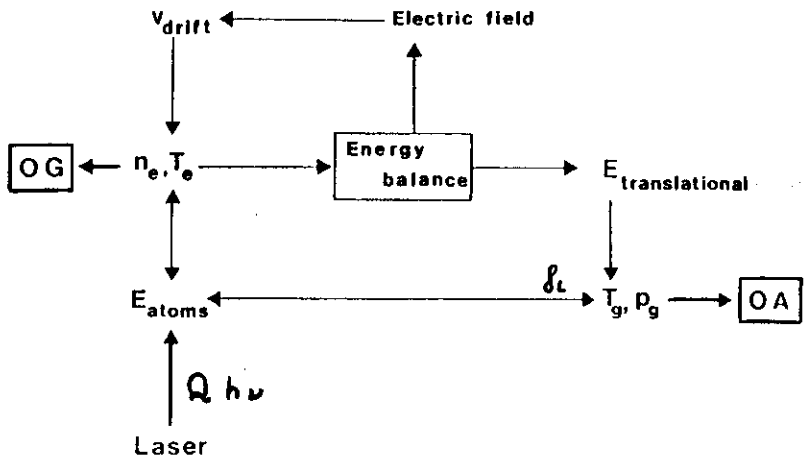

Q photons absorbed per unit time

Input electric power $P_e = i\,E\,l$

current, electric field, length

Energy balance in Ne positive column

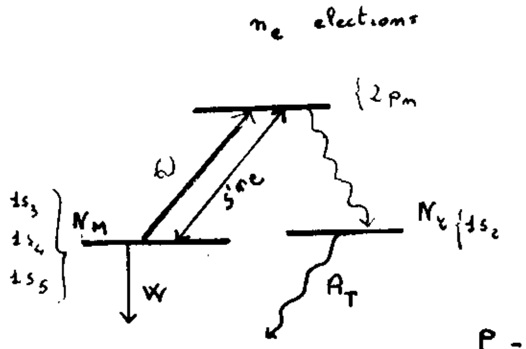

Input power = Electric power + Ω

Dissipated power =

$$P_g + P_r + P_W$$

P_g = gas heating

P_r = visible radiation

P_W = wall deposited energy

$$P_r = \pi R^2 \ell \; S' n_e \; N_M \cdot (2 eV)$$

$P_W = \pi R^2 \ell \; W N_M \cdot (16.6 \text{ eV})$ diffusion of metastables

$+ \pi R^2 \ell \; A_T N_r \cdot (16.7 \text{ eV})$ vuv radiation

$+ \pi R^2 \ell \left[D_a \left(\frac{2.4}{R}\right)^2 \right] n_e \cdot (21.6 \text{ eV})$ recombination

The input power is dissipated into

P_g = gas heating — contributes to 0 A

P_{vis} = visible radiation

P_{uv} = uv radiation — contributes to 0 A

P_{n_e} = wall ion-electron recombination — "

P_M = wall metastable disexcitation — "

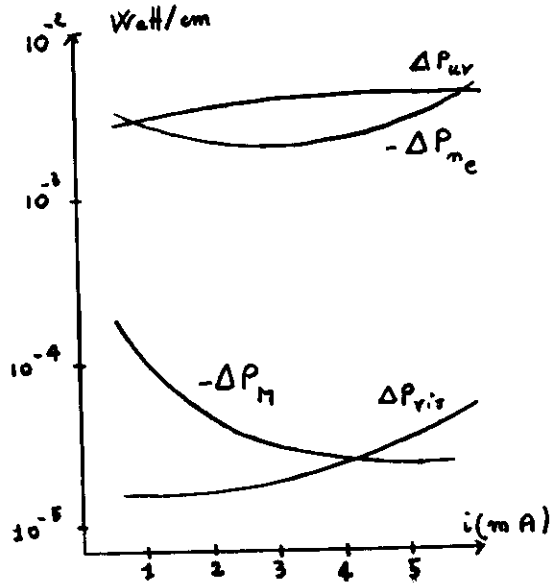

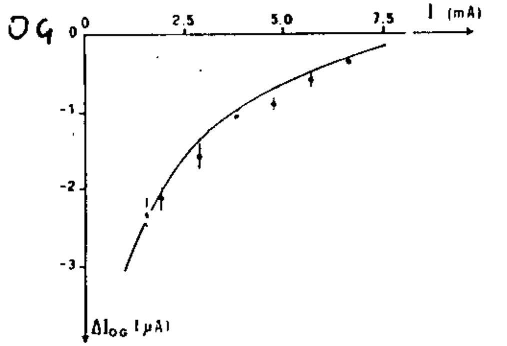

Fig. 3. Optogalvanic signals, with error bars, versus discharge current for the $1s_5$–$2p_4$ neon transition at 1.5 Torr pressure. The theoretical curves have been obtained from the model presented in ref. [2] as explained in the text.

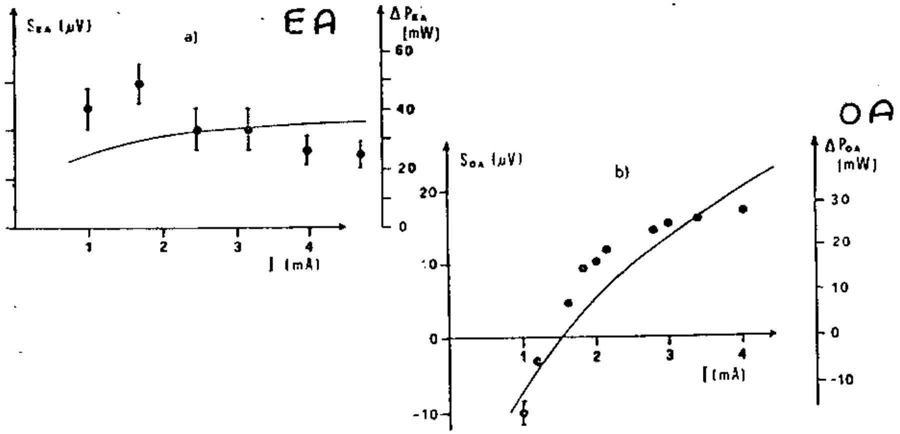

Fig. 2. Experimental results, with error bars, for the EA signals (a), and OA signals (b), versus the discharge current in a 1.5 Torr discharge. Theoretical curves for the internally dissipated power in the voltage modulation, ΔP(EA), and in the optoacoustic observations, ΔP(OA). Modulation voltage applied in the EA experiment was 5 V. Irradiation at 594.5 nm on the $1s_5$–$2p_4$ line was used in the OA observations.

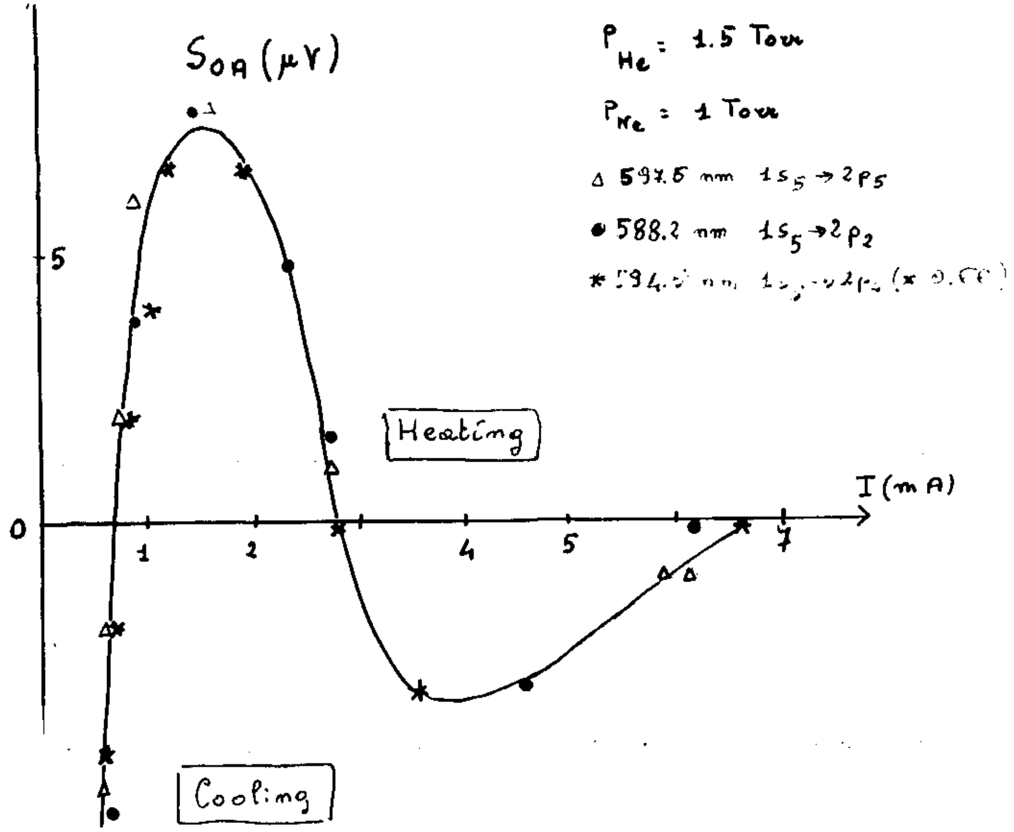

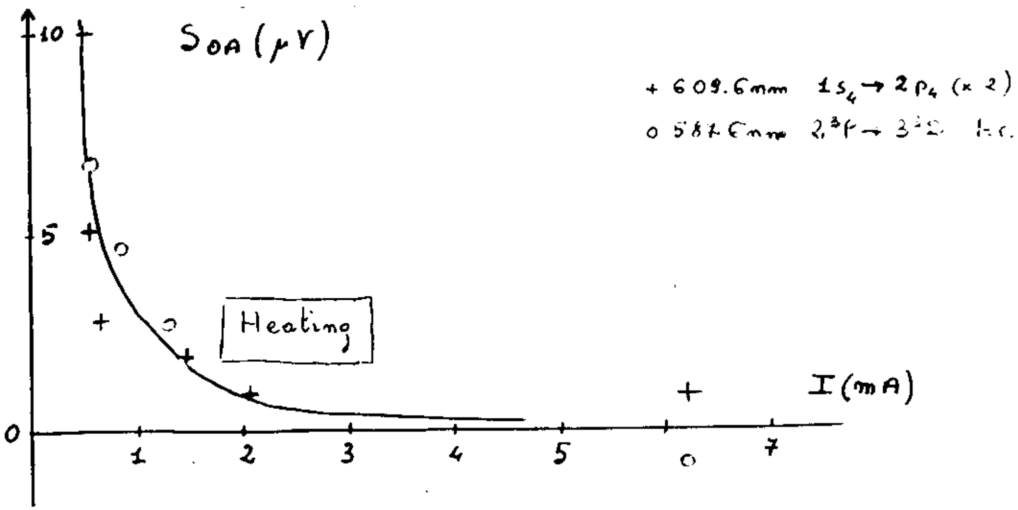

Chaos =

→ deterministic motion

→ associated to few degrees of freedom

→ aperiodic

→ with a large sensitivity on initial conditions

Rayleigh - Benard instability

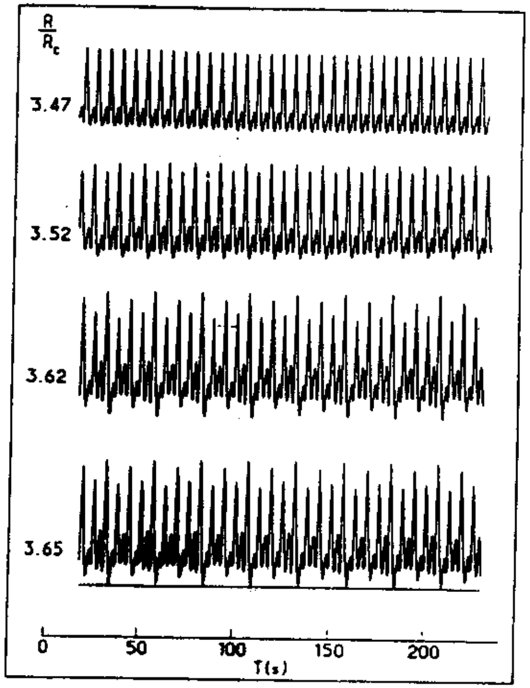

f/4

f/8

f/16

Fig. 2. — Direct time recordings of temperature for various stages of the period doubling cascade showing the onset of f/4 ($R/R_c = 3.52$), f/8 ($R/R_c = 3.62$), f/16 ($R/R_c = 3.65$).

T. Braun et. al P.R.L. 59 613 (1987)

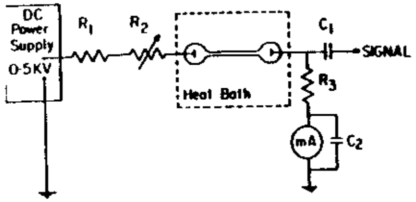

IG. 1. Schematic diagram of the experiment. $R_1=90$ kΩ, -10 kΩ, $R_3=5$ kΩ, and $C_1=C_2=0.01$ μF.

helium lamp

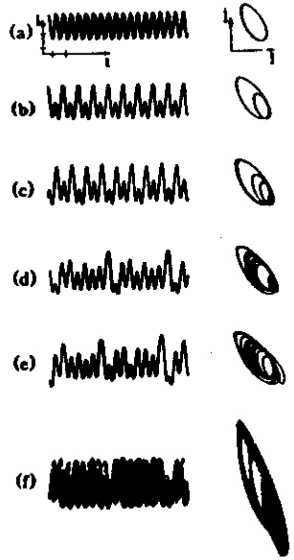

FIG. 2. Experimental results for a helium spectral lamp operating at about 12 mA. Self-generated oscillations of the current $I(t)$ through the lamp are shown on the left with the corresponding phase portraits $dI/dt \times I$ on the right. The current increases from (a) to (f). The scales for $I(t)$ are 0.04 mA/division and 10 μs/division. The phase portrait in (f) is vertically expanded.

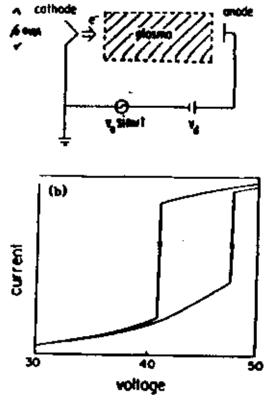

FIG. 1. (a) Schematic of experimental setup. (b) I-V characteristic of anode current, I_a, vs dc anode voltage bias, V_d. The upwards pointing arrow indicates the rapid increase in I_a as V_d is increased and the downwards pointing arrow indicates the rapid decrease in I_a as V_d is decreased.

Anode potential $V_d + V_0 \sin \omega t$

Signal →

FFT transform →

phase-space

Poincaré section

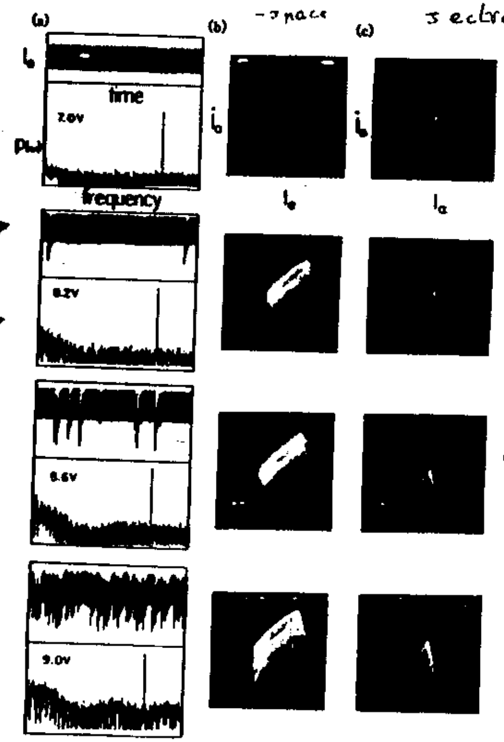

$V_0 = 7$

$V_0 = 8.2$

$V_0 = 8.6$

$V_0 = 9$ Volts

FIG. 2. (a) Real-time signals of I_a oscillations and the corresponding FFT spectra for $V_0=7$, 8.2, 8.6, and 9 V, respectively. The external drive frequency is at $f_0=14.4$ kHz. The vertical scale on each FFT spectrum is logarithmic. (b) Corresponding phase-space plots of $\dot{I}_a$ vs I_a as V_0 is increased. (c) Corresponding Poincaré sections of ...

P.Y. Cheung, S. Donovan and A.Y. Wong

P.R.L. 61 1360 (1988)

VOLUME 57, NUMBER 6 PHYSICAL REVIEW LETTERS 11 AUGUST 1986

Optogalvanic Observation of Ionization Waves in Hollow-Cathode Discharges

Kenji Tochigi
Production Engineering Research Laboratory, Hitachi Ltd., Yokohama 244, Japan

and

Shiro Maeda and Chiaki Hirose
Research Laboratory of Resources Utilization, Tokyo Institute of Technology, Yokohama 227, Japan
(Received 14 April 1986)

pag. 711

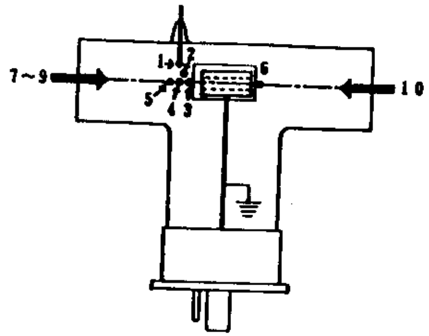

FIG. 1. Directions and positions of the laser illumination. Circles and arrows show, respectively, that the laser beam was directed perpendicular and parallel to the axis of the cathode cylinder, and the attached numbers refer to the first column of Table I.

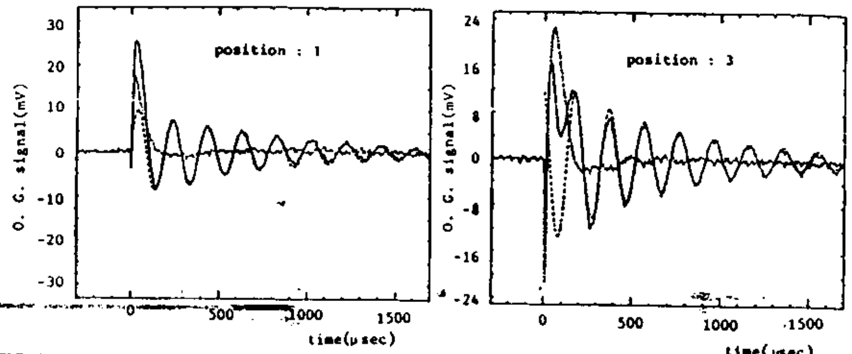

FIG. 2. Transient OG signals of Ne $2p_8$-$1s_5$ line at 633.4 nm (see legend of Fig. 1 for the attached numbers). Solid curves are the observed signals, the dashed lines are the simulated curves, and the dotted curves corresond to the residual, i.e., the observed minus the simulated signals.

Laser induced phase locking
hydrogen plasma striations
[W. Glab and M. N. Nayfeh
A.P.L. 40 574 (1982)]

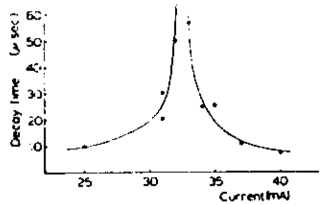

FIG. 2. Decay rate of the laser induced transient as a function of the current in the plasma while keeping the pressure constant.

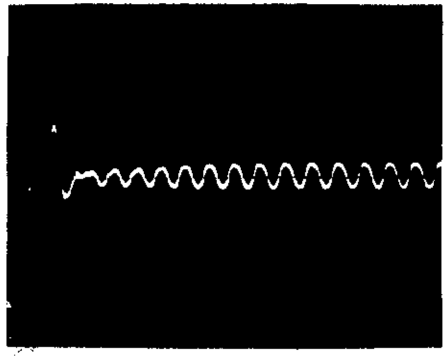

FIG. 4. Oscilloscope trace corresponding to five laser interactions of high intensity with the plasma exhibiting single-mode striation and phase locking. The time base is 10 μs/div.

OG signals by
laser ionization of
hydrogen n=2 → continuum
656.3 nm radiation

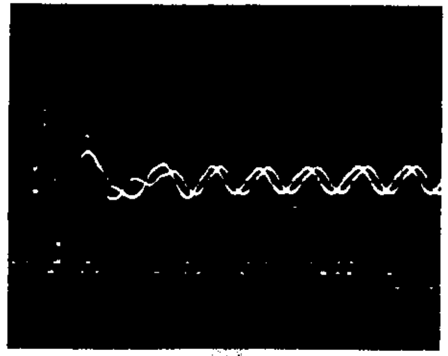

FIG. 3. Oscilloscope trace corresponding to two laser interactions of low intensity showing single-mode striation and random phase.